Journal of Anatomy

J. Anat. (2010) **216**, pp62–79 doi: 10.1111/j.1469-7580.2009.01154.x

The enamel–dentine junction in the postcanine dentition of *Australopithecus africanus*: intra-individual metameric and antimeric variation

J. Braga,[1,2] J. F. Thackeray,[3] G. Subsol,[2,4] J. L. Kahn,[5] D. Maret,[1] J. Treil[1] and A. Beck[6]

[1]*Laboratoire d'Anthropobiologie, Université de Toulouse, France*
[2]*Human Origins and Past Environments Programme, Transvaal Museum, Pretoria, South Africa*
[3]*Institute for Human Evolution, University of the Witwatersrand, Johannesburg, South Africa*
[4]*Laboratoire d'Informatique, de Robotique et de Microélectronique de Montpellier, France*
[5]*Institut d'Anatomie Normale de Strasbourg, France*
[6]*Institut de Médecine et de Physiologie Spatiales, Toulouse, France*

Abstract

We used micro-computed tomography and virtual tools to study metric and morphological features at the enamel–dentine junction and on the outer enamel surface in the postcanine dentition of an exceptionally well-preserved maxilla and mandible of an early hominin. The fossil, Sts 52 from Sterkfontein, South Africa, is attributed to *Australopithecus africanus* and is about 2.5 million years old. For comparative purposes in this exploratory study, we also used micro-computed tomography to analyse the dentition of a common chimpanzee (*Pan troglodytes*), a pygmy chimpanzee (*Pan paniscus*) and three extant humans. Metameric variation of the 3D enamel–dentine junction in the two chimpanzee mandibles was much smaller than in extant humans. Variation in metameric shape was high and complex. Notably, the mandibular metameric variation in extant humans can be greater within individuals, as compared with variation between individuals, with differences in shape appearing greater for M2 compared with M1. We recommend the use of a new approach in which individual metameric variation is systematically assessed before making inferences about differences between fossil hominin species. The fossil hominin examined in this study showed a metameric pattern of mandibular variation in shape that was comparable to the pattern seen in two chimpanzees. This degree of metameric variation appeared relatively small compared with the much larger patterns of variation observed within and between extant humans.
Key words antimeric variation; *Australopithecus africanus*; enamel–dentine junction; *Homo sapiens*; metameric variation; molars; *Pan paniscus*; *Pan troglodytes*; premolars.

Introduction

Advances in micro-computed tomography (micro-CT) and computer-aided tools recently facilitated the first 3D analyses of morphological variation of the enamel–dentine junction (EDJ) (Suwa et al. 2007; Skinner et al. 2008a,b, 2009) in primate molars, a feature that is often intact in worn tooth crowns and that determines closely the gross morphology of the outer enamel surface (OES) (e.g. Kraus, 1952; Butler, 1956; Corruccini, 1987, 1998). Korenhof (1960, 1961), who was one of the pioneers in this research, focused on the EDJ of maxillary molars in fossil and living primates. The EDJ is the earliest feature to take shape in dental development, well before the functional emergence of the tooth, when enamel and dentine are deposited on, respectively, the occlusal and basal surfaces of the basement membrane (*membrana praeformativa*) of the inner enamel epithelium of the enamel organ (Schour & Massler, 1940; Massler & Schour, 1946). The shape of the basement membrane is preserved on the EDJ because it does not remodel once its formation is completed. The morphology of the EDJ has been considered to be useful in identifying hominoid fossil species, determining their phylogenetic relationships (Suwa et al. 2007) and distinguishing some species of Pliocene hominins (Skinner et al. 2008a,b, 2009). However, the morphological and metrical features of the EDJ may be expressed differently in each tooth type of the four morphological classes of teeth (incisors, canines, premolars and molars), hence displaying varying degrees of intra-individual variation. Until now, no research has been performed on three major components of intra-individual

Correspondence
José Braga, Lab. Anthropobiologie, Univ. Toulouse, 37 Allées J Guesde, 31000 Toulouse, France. E: braga@cict.fr

Accepted for publication *16 September 2009*
Article published online *9 November 2009*

morphological and metrical variation in the 3D-EDJ: (i) intra-individual metameric variation (differences in expression of a trait between teeth of the same class, e.g. in molars or premolars, through a postcanine tooth row); (ii) intra-individual antimeric variation (differences between the right and left sides) and (iii) intra-individual inter-trait correlations (simultaneous occurrence of two or more traits in a postcanine row). After observing the OES and root morphology in large samples of extant humans, Dahlberg (1945) introduced the concept of the 'key' tooth for each morphological class. With regard to postcanine teeth, the key tooth was said to be the most mesial member, the most stable tooth in terms of development and evolution with (i) less intra-group (e.g. intra-specific) variation in size and morphology, (ii) the least amount of asymmetry and (iii) the most pronounced expressions of a specific feature. For molars, stability was considered to increase from M3 to M2 and from M2 to M1.

The study of 2D occlusal or cross-sectional differences in molars is not new (Hlusko, 2002; Smith et al. 2006; Olejniczak et al. 2007). The inclusion of a third dimension in the study of EDJ metameric variation has provided interesting results (Skinner et al. 2008a,b). However, the issue of metamerism has not yet been addressed with regard to an assessment of within- and between-individual variation. Here we consider two individuals of the same species ('A' and 'B'), each represented by their first and second permanent mandibular molars, 'M_{1A}, M_{2A}, M_{1B} and M_{2B}', respectively. In practice, current studies of metameric variation do not distinguish the following: intra-individual differences between M_{1A} and M_{2A} or between M_{1B} and M_{2B}, and inter-individual metameric differences between M_{1A} and M_{2B} or between M_{1B} and M_{2A}. Therefore, studies of metameric variation of teeth in general, and of the 3D-EDJ in particular, are based solely on teeth considered as isolated objects that may be (and often are) represented by different sets of individuals. This approach is based on assumptions implying that it is possible to investigate metameric variation with no distinction between intra- and inter-individual components. However, as the pattern of intra-individual metameric variation may not be the same in all individuals of the same species, the observed inter-individual metameric differences may be obscured by as yet unknown variability of intra-individual patterns of metameric variation.

Why should we investigate the patterns of intra-individual metameric variation? This issue was raised in the elegant study of Hlusko (2002) on metameric variation in cross-sections and occlusal images of mandibular molars. She investigated metameric variation in mandibular first and second molars and found distinct patterns in extant humans, as compared with common chimpanzees, gorillas and fossil hominins from Sterkfontein in South Africa. She concluded that ''data on metameric variation may provide information regarding function or developmental processes previously indiscernible from fossil material'' (op. cit., p. 86). Indeed, metameric patterns observed in teeth may result from a common developmental mechanism (for review see Weiss, 1990) and/or from functional constraints associated with the orofacial structure (for review see Cowin & Moss, 2001).

In the case of metameric comparisons in fossil hominids, isolated teeth may not represent the same sets of individuals and the observed metameric differences correspond to the sum of (i) intra-individual metameric variation and (ii) inter-individual variation within each type of tooth of a given class. The issue of the morphological and metrical intra-individual variation of the EDJ has not yet been addressed in complete specimens. It is often acknowledged that this issue would be ideally examined in the case of a careful study of mandibular and maxillary postcanine rows on both sides of individuals preserving much of their dentition and at least part of their craniofacial morphology. After controlling for intra-individual antimeric and metameric variation in the 3D-EDJ, we expect to be in a position to determine with more confidence which 3D-EDJ features carry taxonomically relevant information that can be secondarily examined in isolated teeth in the fossil record. Our study was carried out with the explicit goal of documenting 3D changes in the expression of EDJ metrical and morphological features at all points throughout the premolar and molar rows of a fossil hominin's mandibular and maxillary postcanine dentition. In this study we investigate the metrical and morphological differences between: (i) molar (i.e. first, second and third) and premolar (i.e. third and fourth) types within the same mandibular and maxillary quadrant and (ii) sides within the same arcade. We focus on both dental arcades to investigate, firstly, if both patterns of antimeric and metameric variations are of the same magnitude in mandibular and maxillary arcades and, secondly, if antimeric variation is of the same magnitude between key teeth and their distal counterparts among each postcanine class (i.e. premolars and molars). To attain these objectives we examined the 3D-EDJ of 20 premolars and molars by micro-CT in the entire four postcanine rows of the mandibular and maxillary dentition of Sts 52 (Fig. 1). This specimen from Sterkfontein, South Africa is about 2.5 million years old and it represents *Australopithecus africanus* (Dart, 1925), usually regarded as a dietary generalist.

For comparative purposes, in order to interpret our results obtained from Sts 52 and to address the issue of metameric variation within and between individuals, we also undertook micro-CT analyses of mandibles of one common chimpanzee (*Pan troglodytes*), one pygmy chimpanzee (*Pan paniscus*) and three extant humans (Fig. 2). This allowed us to determine whether the pattern of intra-individual metameric variation observed in Sts 52 is similar to that of extant hominoids selected for this exploratory study, recognizing that sample sizes are as yet still small. We investigate the following patterns.

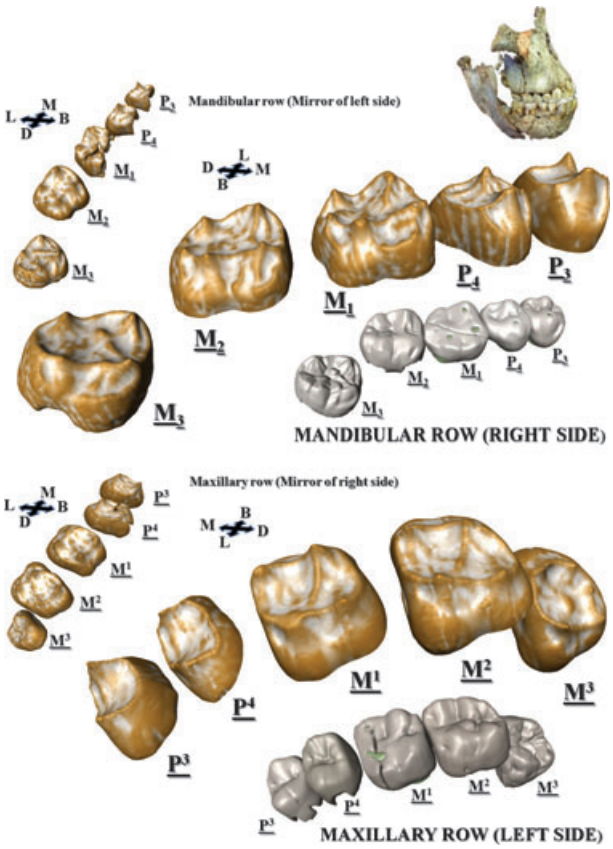

Fig. 1 3D reconstructions and visualizations of the EDJs and OESs (in gray) of the right mandibular and left maxillary rows of an *Australopithecus africanus* specimen (Sts 52, Sterkfontein, South Africa). B, buccal; D, distal; L, lingual; M, mesial. The left mandibular and right maxillary rows are represented with smaller sizes (mirrored from the opposite side) in the upper left of the top and bottom portions of the figure, respectively.

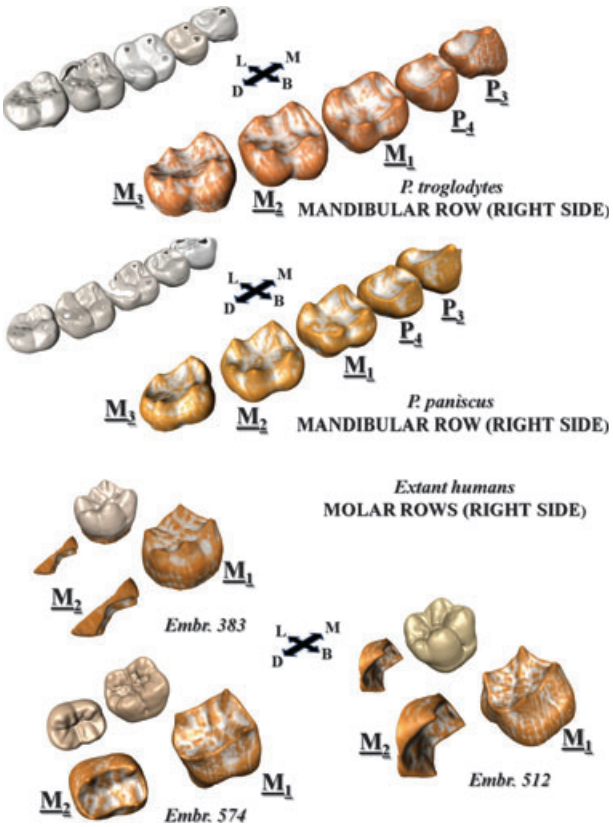

Fig. 2 3D reconstructions and visualizations of the EDJs and OESs (in gray) of the right mandibular premolars and molars for one common chimpanzee (*Pan troglodytes*) and one pygmy chimpanzee (*Pan paniscus*). The EDJs and OESs of the M_{1s} and M_{2s} are also represented for three extant humans (Embr 383, 512 and 574). B, buccal; D, distal; L, lingual; M, mesial.

1 Thepattern of intra-individual metameric variation in all four postcanine classes of *A. africanus* as represented by Sts 52

2 Thepattern of within- vs. between-individual metameric variation in the mandibular first and second molars of three extant humans

3 Thepattern of intra-individual metameric variation in the mandibular molars of one common chimpanzee and one pygmy chimpanzee

Our detailed studies of 3D-EDJ metameric variation in extant human and chimpanzee mandibular molars allow us to determine whether the variation in 3D-EDJ morphology in Sts 52 is regular. More importantly, our analysis allows us to determine, firstly, whether the extant human pattern of 3D-EDJ metameric variation is distinct from that found in two chimpanzee species and, secondly, whether Sts 52 shares the metameric patterns seen in chimpanzees and/or extant humans. We believe that the type of analysis that we present here, with attention to intra-individual and inter-individual components of metameric variation, may improve the identification of its causal mechanisms and may help with the interpretation of the fossil record. We aim to discuss whether this new approach is a prerequisite to improve 3D-EDJ inter-specific comparisons among early hominins.

Materials and methods

Micro-tomographic (micro-CT) record

The following specimens were scanned in 2007 and 2008 in a high-resolution peripheral micro-CT scanner (XtremeCT, Scanco Medical) in the Institut de Médecine et de Physiologie Spatiales, Toulouse, France (http://www.medes.fr/): the maxilla (Sts 52a) and mandible (Sts 52b) of a specimen representing *A. africanus;* three human mandibles from the series of identified skeletons, of known age and sex, from the Institut d'Anatomie Normale de Strasbourg, France, with catalogue numbers Embr 383 (male, 5 years and 4 months old), 512 (male, 4 years and 6 months old) and 574 (female, 5 years and 4 months old); and mandibles of a common chimpanzee (catalogue number 31489) and a pygmy chimpanzee (catalogue number 11149) from the Royal Museum of Central Africa, Tervuren, Belgium (Table 1). Scans were

Table 1 Composition of the study sample.

	P_3 EDJ	P_3 OES	P_4 EDJ	P_4 OES	M_1 EDJ	M_1 OES	M_2 EDJ	M_2 OES	M_3 EDJ	M_3 OES	CT slice no.	Size (Gb)
Sts 52a	2	2*	2	2*	2	2*	2	2*	2	2	2108	19.6
Sts 52b	2	2*	2	2*	2	2*	2	2*	2	2	2716	29.2
Pan troglodytes (31489)	2	2*	2	2*	2	2*	2	2*	2	2*	2834	32.6
Pan paniscus (11149) I	2	2*	2	2*	2	2*	2	2*	2	2*	2637	24.3
Embr 383	–	–	–	–	2	2	2	–	–	–	1750	10.7
Embr 512	–	–	–	–	2	2	2	–	–	–	1800	16.5
Embr 574	–	–	–	–	2	2	2	2	–	–	1730	17.7

One hundred EDJs and OESs were reconstructed in 3D and represent 50 dental crowns in total.
*When the 3D model cannot be used for metrical analysis because of wear and/or preservation status.

performed at an energy level of 40 keV. Pixel dimensions and slice thickness between reconstructed serial images were isometric with a resolution of 41 μm (e.g. isometric voxels of 41 × 41 × 41 μm). Virtual cross-sections were saved in a 32-bit floating-point raw format and finally converted in a 16-bit DICOM format. One hundred dentine and enamel tissues were reconstructed in 3D for 50 dental crowns in total (Table 1, Figs 1 and 2). Twelve of these 50 dental crowns showed no signs of wear (Table 1) and were subsequently used for morphometric analyses of both dentine and enamel 3D surface reconstructions. On account of wear, the enamel caps of 38 remaining teeth were reconstructed in 3D but only the dentine surface was used for morphometric analyses. On account of poor preservation, four teeth were excluded from this study of the EDJ in Sts 52: the left P_3, P_4, M_1 and right P^4.

Image processing and 3D reconstructions

Image stacks converted in an 8-bit TIFF format were imported into the Amira software package (v.5, http://www.amiravis.com) for the segmentation (isolation and digital extraction) of the dentine at the EDJ level and its subsequent 3D visualization. The separation of enamel and dentine was clear enough on the images and the two dental tissues were associated with distinct gray-scale values. As there is no fully automatic segmentation method available as yet, we carried out a semi-automatic segmentation of the micro-CT record (using the following segmentation tools with Amira: 'Magic Wand' and 'Blowtool'). The 3D, triangle-based, surface (or mesh) reconstructions were made using an 'unconstrained smoothing' parameter (with Amira). We simplified each tooth surface to approximately 250 000 faces prior to our comparisons. Morphological details of the EDJs on the right mandibular and left maxillary postcanine row dentitions of Sts 52 are shown in Figs 3 and 4. In this fossil specimen, we used the right mandibular (Fig. 3) and left maxillary (Fig. 4) postcanine rows as templates, or references, because they were better preserved than the opposite side. We studied the EDJ on the opposite side (left mandibular and right maxillary postcanine rows) and mirrored them for a right/left comparison. In all five comparative specimens, we also used the right mandibular postcanine rows as templates (Figs 5 and 6) and mirrored the left ones for comparison (see Supporting Information). Mirroring was performed with the use of Trimesh2, a C++ library and set of utilities for manipulation of 3D triangle meshes (http://www.cs.princeton.edu/gfx/proj/trimesh2).

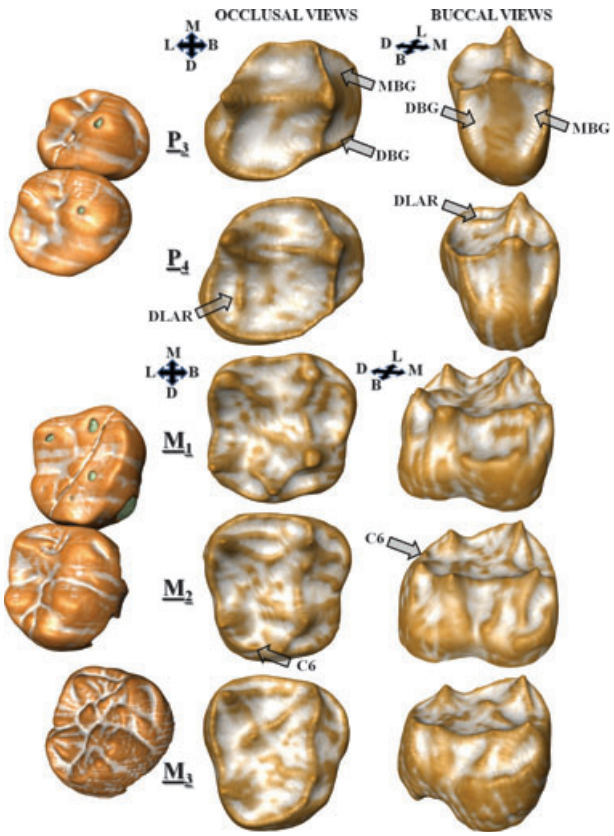

Fig. 3 Morphological features seen in occlusal and buccal views on 3D reconstructions and visualizations of the EDJs and OESs of the right mandibular postcanine row of an *Australopithecus africanus* specimen (Sts 52, Sterkfontein, South Africa). Arrows indicate the main morphological features cited in the text. MBG, mesial buccal groove; DBG, distal buccal groove; C6, tuberculum sextum; B, buccal; D, distal; L, lingual; M, mesial.

Graphic representation

With the use of Amira ('GetCurvature' module), we used the 'shape index' of Koenderink & van Doorn (1992) as a tool in the graphical representation of 3D-EDJ shapes (Figs 1–8). The shape index gives a simple measure of 'local shape' and is scale invariant. It is a number in the range [−1, +1] defined through the principal curvatures. At the extremes of the shape index

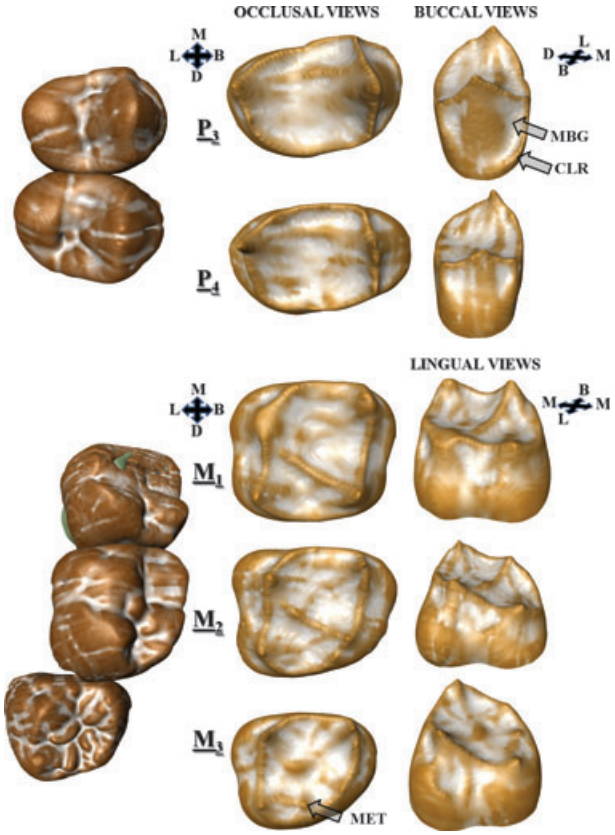

Fig. 4 Morphological features seen in occlusal, buccal and lingual views on 3D reconstructions and visualizations of the EDJs and OESs of the left maxillary postcanine row of an *Australopithecus africanus* specimen (Sts 52, Sterkfontein, South Africa). Arrows indicate the main morphological features cited in the text. MBG, mesial buccal groove; CLR, cingulum-like ridge; MET, metaconule; B, buccal; D, distal; L, lingual; M, mesial.

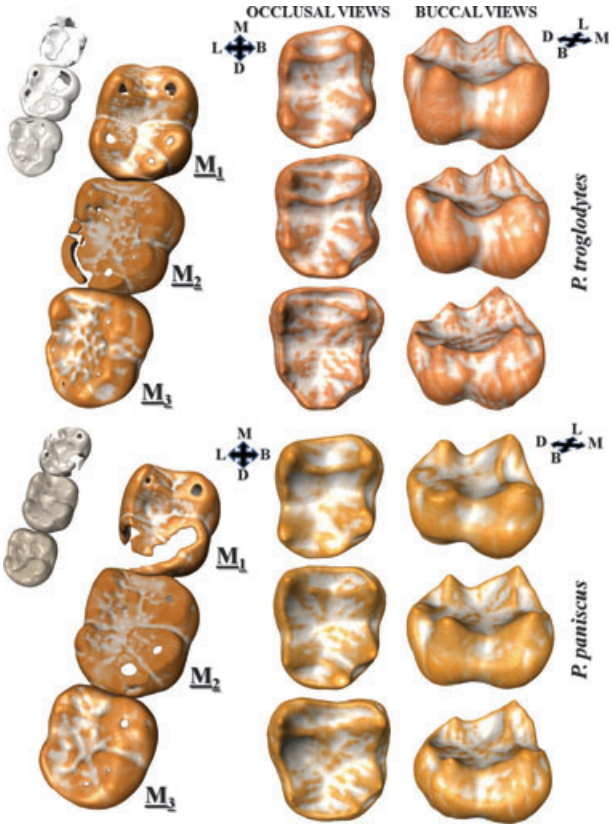

Fig. 5 Morphological features seen in occlusal and buccal views on 3D reconstructions and visualizations of the EDJs and OESs (represented in gray with smaller sizes when mirrored from the opposite side) of the right mandibular molars of two *Pan troglodytes* and *Pan paniscus* specimens. B, buccal; D, distal; L, lingual; M, mesial.

interval, we have concave and convex minima and maxima. A shape index of zero indicates a saddle-like local structure. In all of our figures, the shape index is mapped on a color scale (convex maxima in white; convex maxima in color).

Registration

All comparisons required to study intra-individual metameric and antimeric variations in shape were performed by rigid surface registration (alignment) and scaling (Procrustes superimposition). Each of two surfaces to be matched is described by a set of 3D points. A rigid registration is a displacement '(R, t)' that maps each point of one surface to a corresponding point of the other surface where 'R' is a 3×3 rotation matrix and 't' is a translation vector. The best rigid registration will align two surfaces with the minimal distance between them, by using the 'iterative algorithm' (Besl & McKay, 1992). Therefore, ideally, for an operator-independent registration, as the two surfaces do not come from the same object but from objects of the same class (e.g. teeth), it is highly desirable to establish point-to-point correspondences automatically without any prior choice regarding topology, i.e. without any selection of a specific landmark that may influence the results. Indeed, detailed analysis of anatomical shape variability depends on the selection of corresponding points on specific areas of different shapes. In the case of right/left registration to visualize morphological differences between antimeres (see Supporting Information), as the 3D-EDJs to be compared were very similar, we aligned (rigid registration with scaling) the mirrored mesh and template, or reference (on the right mandibular and left maxillary postcanine rows), by matching the two meshes using the overlapped region found automatically with the use of the Rapidform software (http://www.rapidform.com). In the case of Procrustes superimpositions of EDJs within the same class and quadrant to quantify metameric variations in shape, for alignment of the P4s and P3s, M1s and M2s, M2s and M3s, and a subsequent principal component (PC) analysis (see below; Figs 7–11), we used 40 semi-landmarks equally spaced on the marginal ridges between the tips of the main dentine horns (DHs). The locations of these semi-landmarks were calculated with the use of Rapidform software. Because of the presence of slight dentine wear on some EDJs, we did not use the tips of the DHs as homologous points. For mandibular premolars, we placed 10 and 20 semi-landmarks between the lingual and buccal DHs, respectively, on the mesial and distal marginal ridges. We added 10 semi-landmarks on the essential crest that connects the two DHs. For maxillary premolars, we placed 20 semi-landmarks between the lingual and buccal DHs, on both mesial

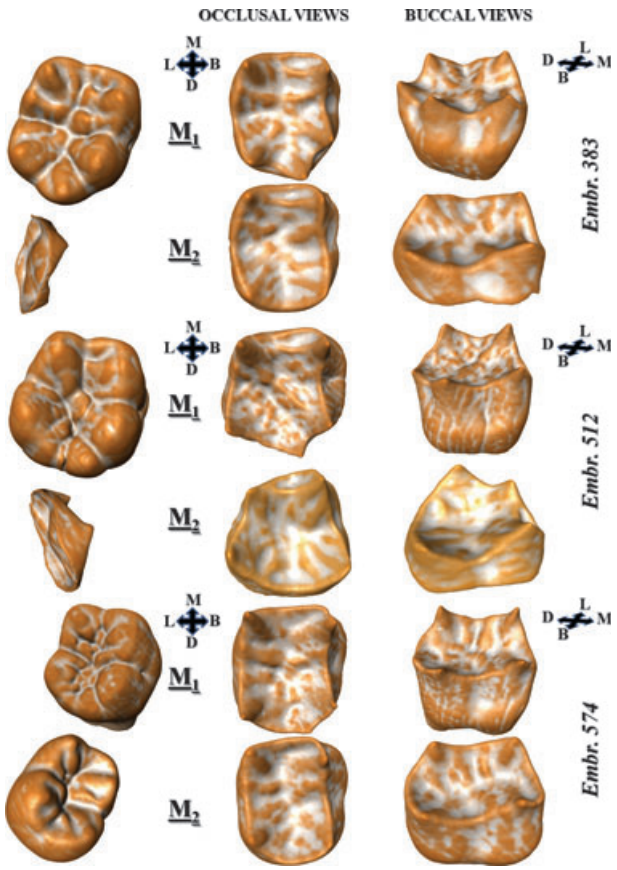

Fig. 6 Morphological features seen in occlusal and buccal views on 3D reconstructions and visualizations of the EDJs and OESs of the right M_{1s} and M_{2s} of three extant humans. B, buccal; D, distal; L, lingual; M, mesial. (The OESs of individuals numbered Embr 383 and 512 are not fully formed and are not represented.)

and distal marginal ridges. For both mandibular and maxillary molars, we placed 10 semi-landmarks on each of the four ridges located between the mesio-lingual, mesio-buccal, disto-lingual and disto-lingual cusps (the hypoconulid was not used on mandibular molars).

Morphological traits on the EDJ

We examined the morphological features on the EDJ of both mandibular and maxillary postcanine teeth of Sts 52 (20 premolars and molars in total) (Figs 3 and 4; Table 1), mandibular postcanine teeth of chimpanzees (two mandibles) (Fig. 5; Table 1), and M_1 and M_2 of extant humans (three mandibles) (Fig. 6; Table 1). Many of these dental morphological traits were scored using the Arizona State University Dental Anthropology System, which comprises a set of rank-scale reference plaques and procedures to standardize observations in the OES of the permanent dentition (Turner et al. 1991). All features reported in this study have already been defined and described elsewhere in great detail on the OES (e.g. Hillson, 1996; Scott & Turner, 1997). Here, we described only the variants of these features that we observed on Sts 52. They have been considered as useful taxonomic discriminators, especially in distinguishing robust from non-robust forms (e.g. Wood & Abbott, 1983; Wood et al. 1983; Suwa, 1988). Of the features investigated here, only four morphological traits of mandibular molars have been subject to a careful inspection at the EDJ level (Skinner et al. 2008a).

Shape variation in 3D-EDJ

The study of antimeric and metameric intra-individual variation in shape was completed by Procrustes superimposition of the semi-landmark configurations. We then employed a PC analysis to identify independent (uncorrelated) linear combinations of geometric semi-landmark shifts (warps). We plotted, separately for the mandibular and maxillary molars, the PC scores of each EDJ in order to illustrate the aspects of shape differences that covary within the shape space (O'Higgins, 2000). Antimeric and metameric size differences were calculated using the centroid size (CS), the square root of the sum of the squared distances among the landmarks in a configuration, and their center of mass.

Measurements

In order to provide simple and easy-to-use descriptive measurements for further inter-specific and intra-specific comparative analyses using more specimens, we added metrical data to our observations on mandibular molars (see Supporting Information). These measurements allowed us to determine how the relative locations of the different DHs contributed to the metameric variation between mandibular molars. We measured the 3D (non-projected) five angles formed by three specified points selected on the apices of the main mandibular molar DHs: at the level of the protoconid, metaconid, hypoconid, entoconid and hypocolunid DHs (Fig. 12).

Results

The OES and some patterns of metameric variation have been described in detail by Robinson (1956) regarding the dentition of Sts 52. The mandibular and maxillary first permanent molars, and the mandibular premolars, are worn to the point where very small dentine patches expose the DHs (Fig. 1). All of the other postcanine teeth are slightly or moderately worn, except the third mandibular and maxillary molars, which are not in occlusion (Figs 1, 3 and 4). The developing M_1 and M_2 of these specimens are still embedded in bone, allowing the analysis of both their EDJs and totally unworn enamel caps (Figs 2 and 6). The common and pygmy chimpanzee mandibles represent adult specimens with their M_3 into functional occlusion and with all of their postcanine teeth showing moderate to important degrees of wear (Figs 2 and 5).

The mandibular postcanine row in Sts 52 (*A. africanus*)

We first describe the right mandibular postcanine EDJs because this side is best preserved (Figs 1, 3 and 7). These

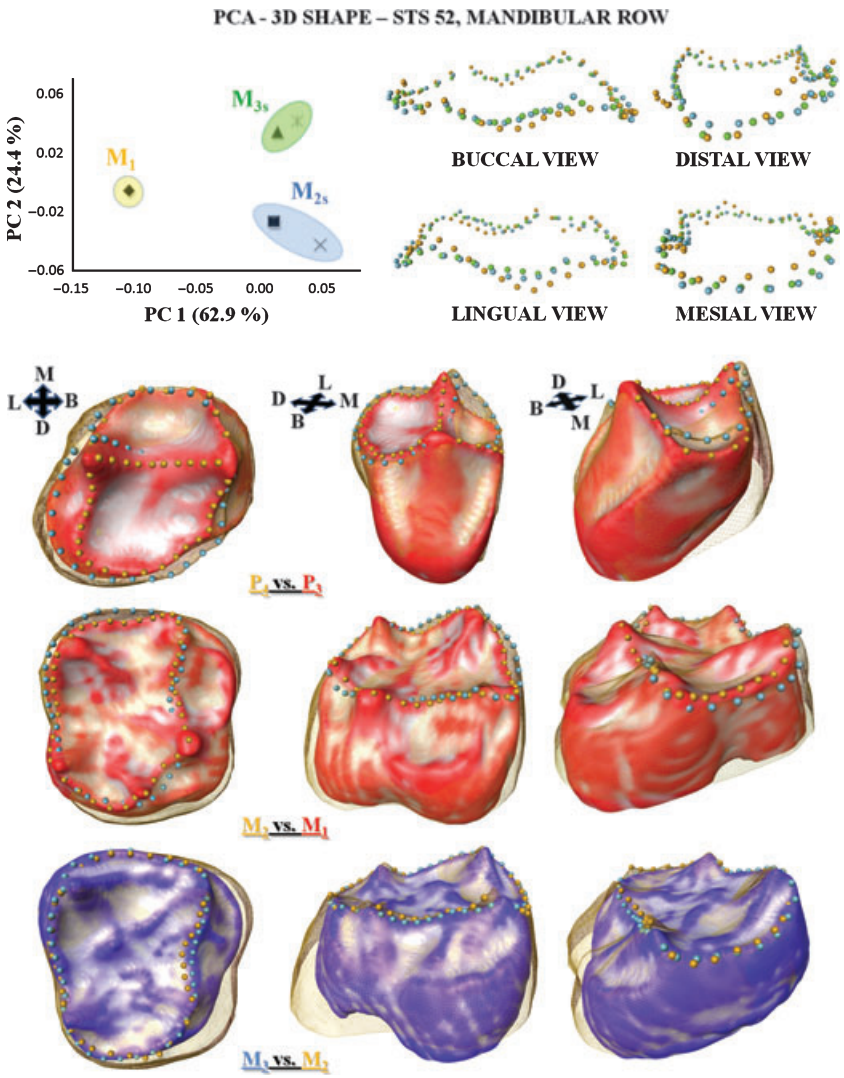

Fig. 7 Shape variability of the EDJ marginal ridges on the mandibular molars of an *Australopithecus africanus* specimen (Sts 52, Sterkfontein, South Africa). The top left graph represents a PC analysis of the semi-landmark configurations. PC1 and PC2 represent PCs of shape variation resulting from relative warp analysis (PC3 accounts for only 7.7% of variation). Right metameric variation is illustrated by the Procrustes superimposition of the RP_4 (yellow) and RP_3 (red), the RM_1 (red) and RM_2 (yellow), and the RM_2 (yellow) and RM_3 (blue). For these alignments, we used 40 semi-landmarks equally spaced on the marginal and essential ridges between the tips of the main DHs. The four top right views represent the semi-landmarks after Procrustes superimposition of all three right mandibular molars. B, buccal; D, distal; L, lingual; M, mesial.

mandibular right EDJs are subsequently compared with the left (L) ones (see Supporting Information).

The 3D-EDJ intra-individual metameric mandibular premolar variation (right side) is strong for most of the recorded morphological features (Figs 3 and 7). This has been previously noted by Robinson (1956) at the OES. Both right mandibular premolars show well-developed and uninterrupted mesial and distal marginal ridges with near equal protoconid and metaconid DHs. Both right mandibular premolars also show marked mesial and distal buccal grooves on the buccal face (Fig. 3). Seen in occlusal view, the essential cresting pattern varies from RP_3 to RP_4. On the RP_3, a prominent, straight and uninterrupted essential crest connects the two DHs. This buttress runs through the center of the occlusal surface and delineates well the distinct mesial and distal occlusal fossae. On the RP_4, the mesial and distal fossae are not well separated. A single buttress arises from the protoconid DH and runs down into the occlusal basin where it ends. The lingual buttress bifurcates down and buccal to the metaconid DH into the center of the occlusal surface where it ends. A third buttress runs down from the protoconid DH but in a distal direction where it forms a well-developed distolingual occlusal accessory ridge on the lingual part of the distal fossa and can also be seen at the OES (Fig. 3). This distolingual accessory ridge does not reach the distal marginal ridge, is only present on the RP_4 (Fig. 3) and should not be confused with the 'tendency to cuspule formation', which has also been described on the rear wall of the posterior fovea, at the OES, in some *A. africanus* P_4s from Sterkfontein (Robinson, 1956) and which we did not observe on the EDJ. The Procrustes superimposition of the RP_4 (CS = 19.1) and RP_3 (CS = 17.1) shows marked differences in both mesiolingual angle and distal margin, which are significantly enlarged in the former EDJ (Fig. 7). Moreover, there is a mesial shift of the metaconid relative to the protoconid on the RP_4, in comparison to the RP_3 (Fig. 7).

There is marked EDJ metameric variation on the right mandibular molar row and the degree of correspondence

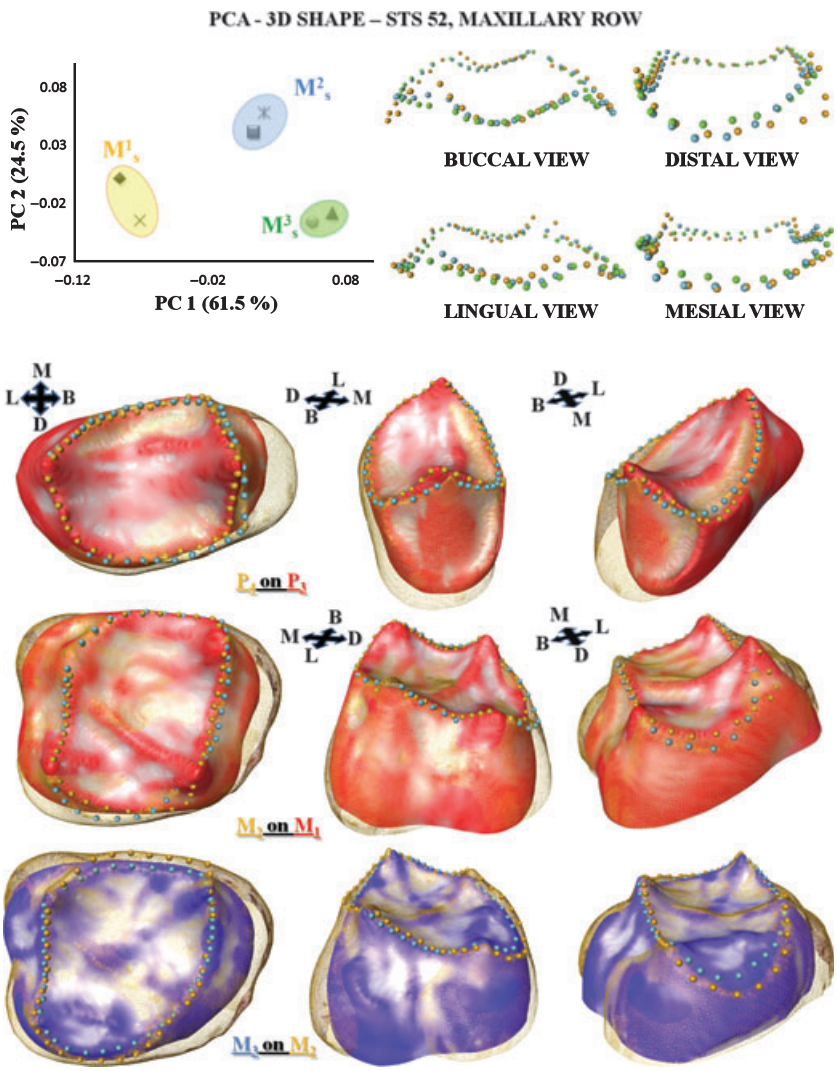

Fig. 8 Shape variability of the EDJ marginal ridges on the maxillary molars of an *Australopithecus africanus* specimen (Sts 52, Sterkfontein, South Africa). The top left graph represents a PC analysis of the semi-landmark configurations. PC1 and PC2 represent PCs of shape variation resulting from relative warp analysis (PC3 accounts for only 8.3% of variation). Left metameric variation is illustrated by the Procrustes superimposition of the LP^4 (yellow) and LP^3 (red), the LM^1 (red) and LM^2 (yellow), and the LM^2 (yellow) and LM^3 (blue). For these alignments, we used 40 semi-landmarks equally spaced on the marginal ridges between the tips of the main DHs. The four top right views represent the semi-landmarks after Procrustes superimposition of all three left maxillary molars. B, buccal; D, distal; L, lingual; M, mesial.

between OES and EDJ morphology can be recorded only in part (Figs 1 and 3). The OES morphology does not allow a description of metameric variation throughout the complete molar row as the enamel cap of the M_1 is too worn to assess discrete traits (Figs 1 and 3). We note an increasing degree of expression of the EDJ trigonid crest patterning from the M_1 to the M_3. This mesial to distal manifestation ranges from (i) well-pronounced but separated crests on the distal slopes of the protoconid and metaconid DHs towards the occlusal basin (RM_1), (ii) two parallel, uninterrupted crests linking both mesial and distal aspects of the protoconid and metaconid DHs and delineating an oval shape basin (RM_2), and (iii) three uninterrupted crests delineating a triangle-shaped basin and connecting the protoconid, the metaconid DHs and a small dentine cusplet located distally towards the occlusal basin (RM_3), which can also be seen at the OES (Fig. 3). Protostylid expression at the EDJ is marked from the M_1 to the M_3. In all instances, a crest-like feature is clearly visible on the mesial side of the protoconid DH and a crest runs from the hypoconulid DH towards the buccal face (Fig. 3). In the first molar, this mesial crest does not connect with another, marked and distally placed crest that connects the protoconid to the hypoconid DH to form a buccal basin. By contrast, in the RM_3, a crest lies on most of the middle part of the buccal face and extends from the distal to the mesial side of the protoconid DH. This crest is associated with a vertically-oriented wrinkle also located on the middle part of the buccal face, between the protoconid and hypoconid DHs. The RM_2 displays almost the same protostylid expression as that of the RM_3, with only a slight difference; the crest lying on the mesial side of the protoconid DH does not extend much on the middle part of the buccal face where there is only the transversally-oriented wrinkle already observed on the RM_3. The C6 is expressed only on the RM_2 in the form of an independent and small DH visible on the marginal ridge of the distal fovea between the hypoconulid and entoconid DHs (Fig. 3) (the 'fovea-type C6' recorded by Skinner et al. 2008a). None of the three lower molar EDJs display a C7. We plot only the first two PCs in the analysis of the configuration of semi-landmarks to

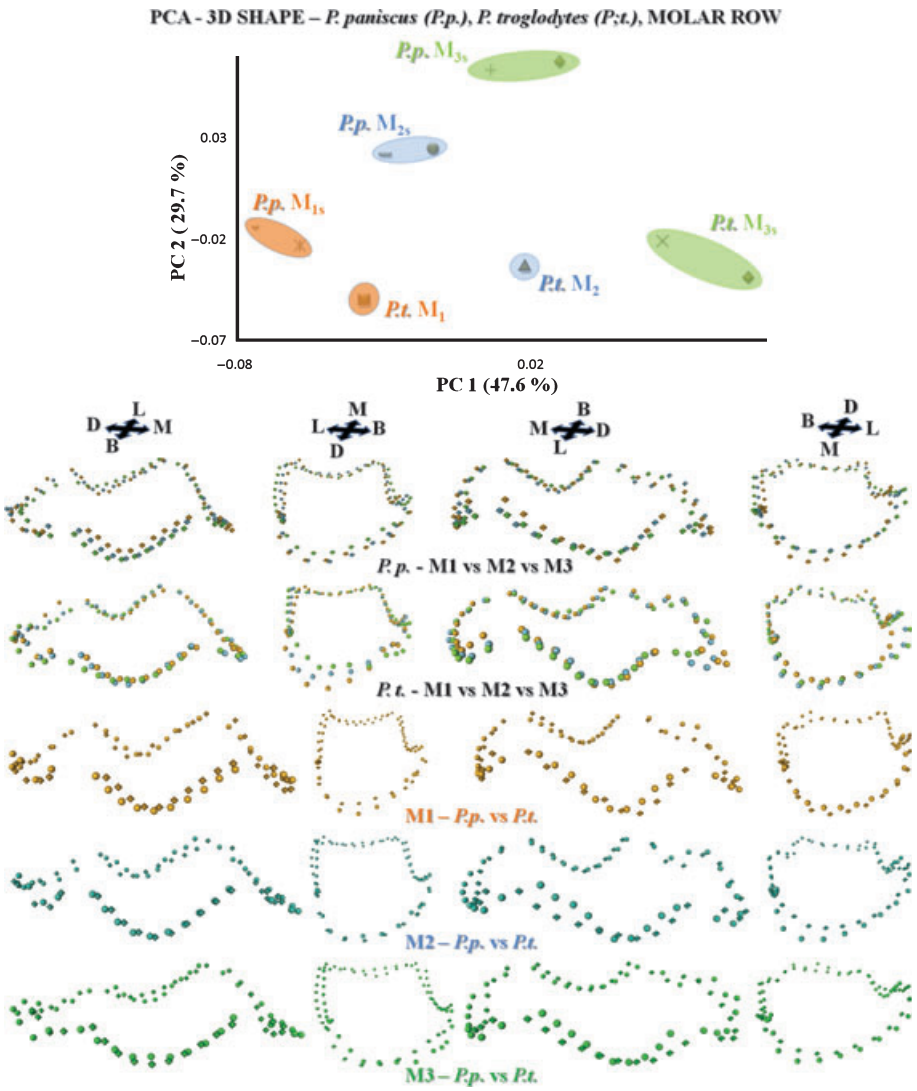

Fig. 9 Shape variability of the EDJ marginal ridges on the mandibular molars of two *Pan troglodytes* (*P.t.*) and *Pan paniscus* (*P.p.*) specimens. The top graph represents a PC analysis of the semi-landmark configurations. PC1 and PC2 represent PCs of shape variation resulting from relative warp analysis (PC3 accounts for only 7.7% of variation). For the Procrustes superimpositions, we used 40 semi-landmarks equally spaced on the marginal and essential ridges between the tips of the main DH. B, buccal; D, distal; L, lingual; M, mesial. Right metameric variation is illustrated by the Procrustes superimposition of the RM_1 (brown), RM_2 (blue) and RM_3 (green) semi-landmarks (diamonds, *Pan paniscus*; circles, *Pan troglodytes*).

reveal differences in shapes between mandibular molars. Indeed, PC1 accounts for 62.9% of the variation, primarily separating the right M_1 vs. both M_{2s} and M_{3s} (Fig. 7). The second PC accounts for 24.4% of the variation and separates the M_{2s} from the M_{3s} (Fig. 7). The third PC accounts for 7.7% of the variation. The Procrustes superimposition of the RM_2 (CS = 26.3) and RM_1 (CS = 25.6) shows a significant mesiolingual elongation in the former, with mainly an enlargement of both its mesiolingual and distobuccal angles, and a sagging of the mesial marginal ridge on the RM_2, which is located lower than the distal crest of the trigonid complex (Figs 3 and 7) (in the M_1, the mesial marginal ridge is located much higher than the trigonid crests). The main changes in shape configuration are indicated by higher scores on PC1 (Fig. 7). The registration of the RM_3 (CS = 27.2) and RM_2 shows less difference, and the same PC1 scores. The higher scores on PC2 for the RM_3 correspond, in comparison to the RM_2, to a significant reduction of the buccal part of the EDJ mainly at the level of the distobuccal angle, a lowering of the buccal DHs (both protoconid and hypoconid) not noticed on the lingual part (Fig. 7).

The antimeric mandibular postcanine morphological variation is faint as indicated after registration (see Supporting Information). The buccal face of the crown is missing on the two premolars and on the first permanent molar. Importantly, the distolingual occlusal accessory ridge is also well developed on the LP_4 and absent on the LP_3 (mirrored in

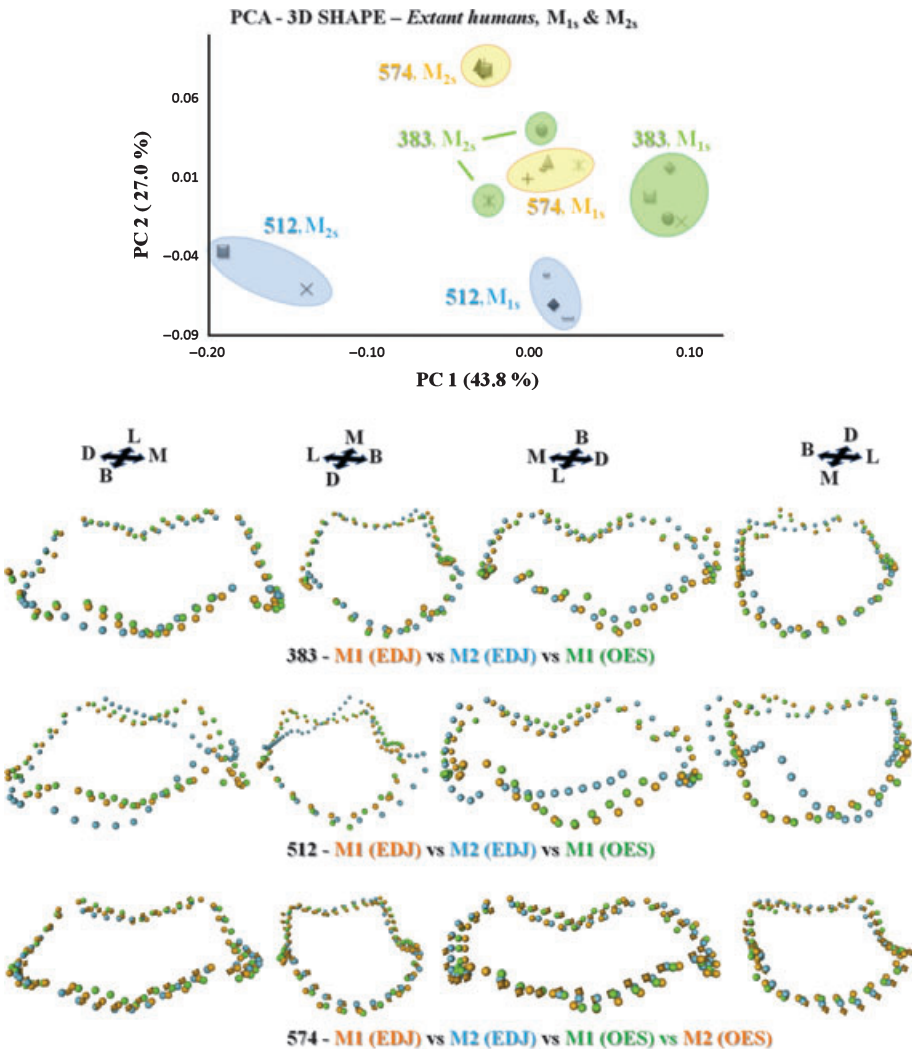

Fig. 10 Shape variability of the EDJ and OES marginal ridges on the M_{1s} and M_{2s} of three extant humans. The top graph represents a PC analysis of the semi-landmark configurations. PC1 and PC2 represent PCs of shape variation resulting from relative warp analysis (PC3 accounts for only 10.2% of variation). For the Procrustes superimpositions, we used 40 semi-landmarks equally spaced on the marginal and essential ridges between the tips of the main DH. B, buccal; D, distal; L, lingual; M, mesial. Right metameric variation is illustrated by the Procrustes superimposition of the RM_1 EDJ (circles in brown), RM_2 EDJ (blue), RM_1 OES (green) and RM_2 OES (diamonds in brown).

Supporting Information). The C6 is expressed on both LM_2 and LM_3, always in the form of an independent and small DH visible on the marginal ridge of the distal fovea between the hypoconulid and entoconid DHs (mirrored in Supporting Information). The PC analysis confirms that metameric variation (both M_1 vs. M_2 and M_2 vs. M_3) is much higher than antimeric variation, which decreases in the M_{3s}, as indicated by less difference on PC2 scores in comparison to the M_{2s} (Fig. 7).

The maxillary postcanine row in Sts 52 (A. africanus)

We first describe the left maxillary molar EDJs because this side is better preserved (Figs 1, 4 and 8). These upper left EDJs will subsequently be compared with the right ones (see Supporting Information).

Both maxillary premolars display well-defined grooves on their buccal face, as noted by Robinson (1956) at the OES. The LP^3 is clearly distinct in having its mesial buccal groove delimited on its outer margin by a cingulum-like ridge running from the mesiobuccal angle of the occlusal face of the crown towards the cervical line (Fig. 4). Seen in occlusal view, both maxillary left premolars display well-developed mesial and distal marginal ridges with a slight transverse crest dividing the occlusal surface into mesial and distal fossae. However, the LP^3 is distinctive in having its marginal ridge interrupted by a faint groove, at mid-distance between the protocone and paracone DHs (Fig. 4). Whereas the LP^4 displays near equal protocone and paracone DHs, the latter is slightly more prominent in the LP^3. The Procrustes superimposition of the RP^4 (CS = 20.0) and RP^3 (CS = 19.5) shows marked differences with a significant

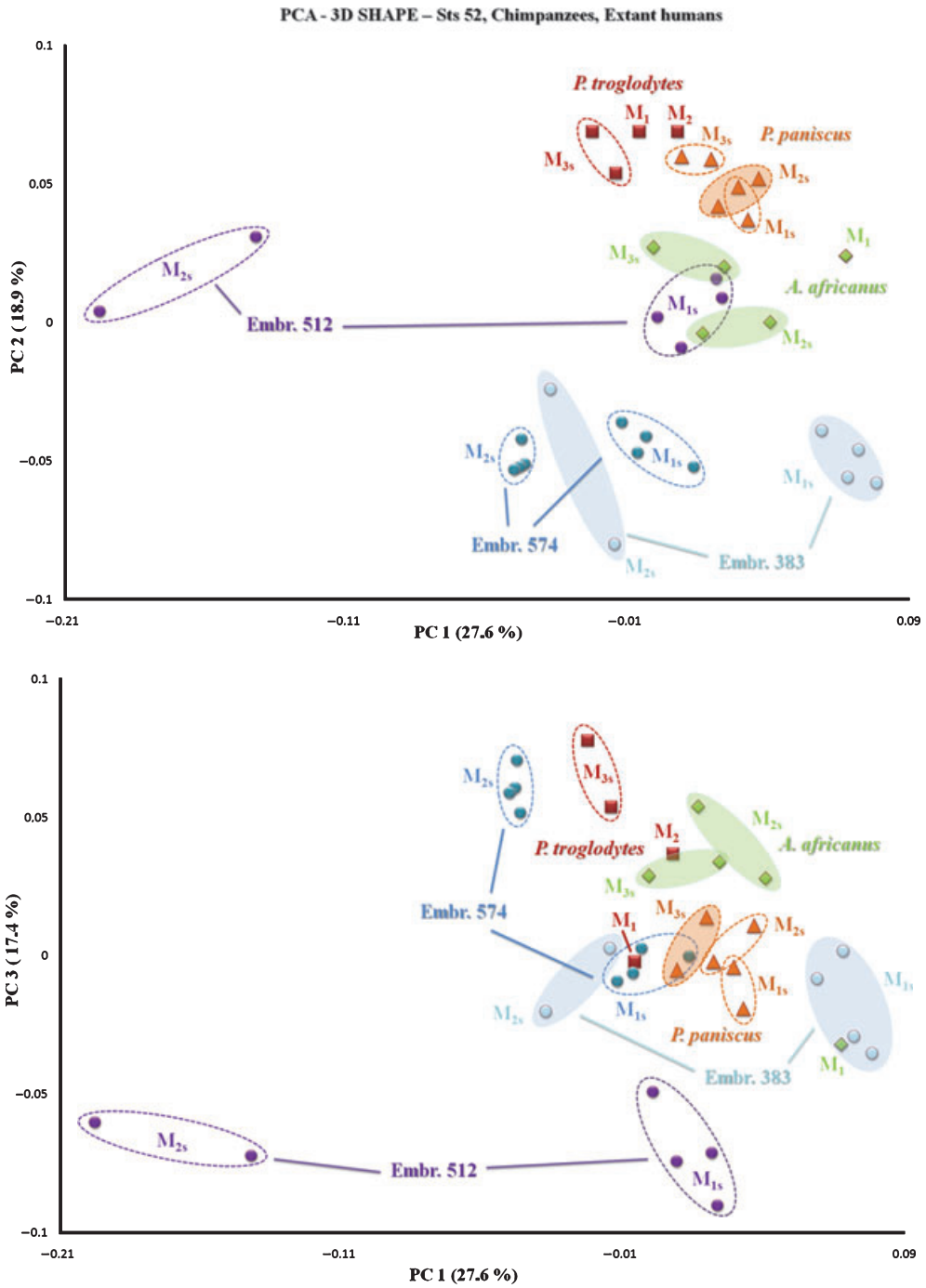

Fig. 11 Shape variability of the EDJ and OES marginal ridges on the right mandibular molars of an *Australopithecus africanus* specimen (Sts 52, Sterkfontein, South Africa), two *Pan troglodytes* and *Pan paniscus* specimens, and three extant humans (numbered Embr 383, 52 and 574). The two graphs represent a PC analysis of the semi-landmark configurations. PC1 and PC2 (top graph) as well as PC1 and PC3 (bottom graph) represent PCs of shape variation resulting from relative warp analysis (PC4 accounts for only 7.6% of variation).

expansion of the buccal face in the former EDJ and a mesial shift of its protocone DH (Fig. 8).

The first and second upper molars have four main cusps with the protocone and metacone DHs linked by a well-developed and uninterrupted oblique ridge (or crista obliqua) separating central and distal fossae (Fig. 4). At first glance, the upper third molar distinctly displays a small distal dentine cusplet (the metaconule DH) with no oblique ridge but, instead, a small central elevation in the central part of the occlusal surface (Fig. 4). This feature may

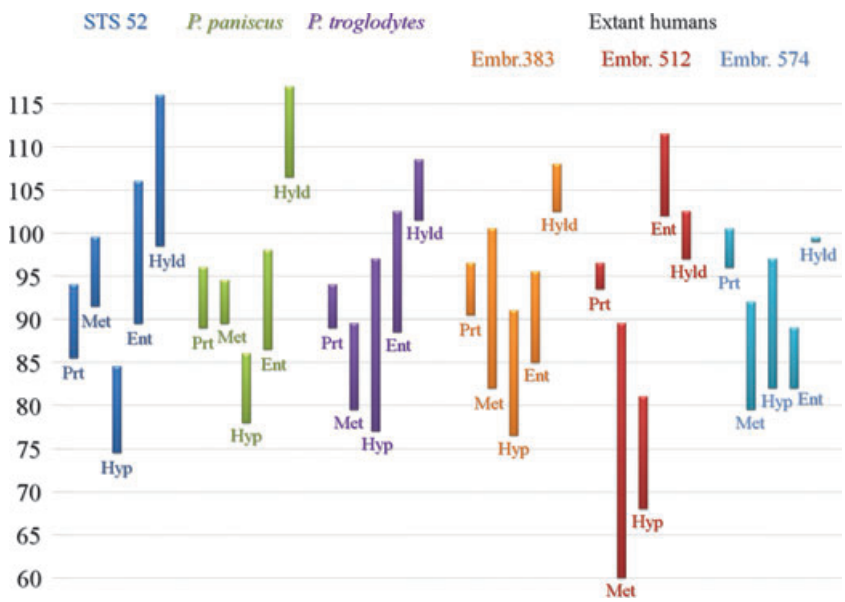

Fig. 12 Variations of the 3D non-projected angles (in degrees) measured at the level of the apices of the main DHs on the mandibular molars (Prt, protoconid; Hyp, hypoconid; Ent, entoconid; Met, metaconid; Hyld, hypocolunid) of an *Australopithecus africanus* specimen (Sts 52, Sterkfontein, South Africa), two *Pan troglodytes* and *Pan paniscus* specimens, and three extant humans (numbered Embr 383, 52 and 574).

correspond to what Robinson (1956) recorded on some Sterkfontein maxillary OES of upper molars as a subdivision of the hypocone into two subequal parts. None of the upper molars show either a Carabelli's DH or a mesial marginal tubercle. We plot only the first two PCs in the analysis of changes in the configuration of semi-landmarks in order to reveal differences in shapes between maxillary molars. Indeed, the first PC accounts for 61.5% of the variation. As for the mandibular molars, PC1 primarily separates the M^{1s} vs. both M^{2s} and M^{3s} (Fig. 8). The second PC accounts for 24.5% of the variation and separates the M^{2s} from the M^{3s} (Fig. 8). The third PC accounts for 8.3% of the variation. The Procrustes superimposition of the LM^2 (CS = 26.5) and LM^1 (CS = 25.4) shows important changes in shape, as indicated by higher scores on PC1 (Fig. 8). In the M^2, there is a significant enlargement of the buccal face, distolingual and mesiolingual angles, associated with a sagging of the distal marginal ridge (Figs 4 and 8). The registration of the LM^3 (CS = 25.1) and LM^2 also shows important differences with higher PC1 scores and lower PC2 scores for the former indicating mainly a flattening of its buccal DHs (in particular the hypocone) and a significant reduction of its mesial and buccal faces and, to a lesser extent, of its disto-lingual angle (Fig. 8). Interestingly, contrary to the mandibular arcade in which CS increases from the M_1 to the M_3, in the maxillary arcade, CS increases from the M^1 to the M^2 and then decreases from the M^2 to the M^3.

As in the case of the mandibular arcade, the alignment indicates that antimeric maxillary postcanine morphological variation is faint (see Supporting Information). The PC analysis indicates that metameric variation (both M^1 vs. M^2 and M^2 vs. M^3) is much higher than antimeric variation, which decreases in the M^{2s} and M^{3s}, in comparison to the M^{1s} (Fig. 8). The mesiobuccal angle of the RP^4 is broken. Importantly, the cingulum-like ridge (Fig. 4) is also well developed on the outer margin of the mesial buccal groove of the RP^3 only (Fig. 8). The marginal ridge of the RP^3 is not interrupted by a groove (see Supporting Information). The RM^3 also displays a metaconule DH but no central elevation (see Supporting Information).

The mandibular molar row in the two chimpanzee species: within- vs. between-species metameric variation

We describe the right mandibular molar EDJ of the two chimpanzee mandibles representing the two species of this genus (*P. paniscus* and *P. troglodytes*) (Figs 2 and 5). These right and left mandibular EDJ data are compared. We focus our descriptions on the molars as the metameric variation of the chimpanzee premolar OES is well known and of limited value for this study because the chimpanzee P_3, with its single dominant cusp, is not comparable to any extant human or *A. africanus* P_3. Indeed, as seen on both chimpanzee premolar EDJs (see Supporting Information), the P_3 has an ovoid occlusal margin, with the long axis running mesiobuccally to distolingually. The large and dominant protoconid DH is located in the center of the tooth. Two buttresses arise from the protoconid DH and run distally to form a distobuccal and a distolingual occlusal ridge. These two ridges meet the distal ridge where they form two tiny tubercles distally. In the *P. troglodytes* individual, two faint dentine ridges are visible at the level of the mesiolingual angle. They delimit a small triangular basin inclining strongly in a lingual direction (see Supporting Information). In the *P. paniscus* individual, a sharp mesiolingual ridge runs downwards from the protoconid DH. A distolingual occlusal ridge inclines strongly in a mesiolingual direction (see Supporting Information). The EDJ of the P_4 for both species of chimpanzee is bicuspid with two small

distobuccal and distolingual dentine cusplets (see Supporting Information). In *P. troglodytes* the protoconid DH (lightly worn) is larger and taller than the metaconid DH, whereas in *P. paniscus*, these are subequal in size, with the protoconid DH being taller. In both species, the mesial and distal occlusal ridges are rounded and the transverse crest is continuous (see Supporting Information).

The 3D-EDJ intra-individual metameric mandibular molar variation (right side) is limited for most of the recorded morphological features (Figs 2 and 5). The degree of correspondence between OES and EDJ morphology can be recorded only in part as both M_1 and M_2 enamel caps show moderate to important wear (Fig. 2). In *P. troglodytes*, we note a small degree of variation in mesial to distal expression of the EDJ trigonid crest patterning (Fig. 5). From the RM_1 to the RM_3, we observe two parallel, uninterrupted crests linking both mesial and distal aspects of the protoconid and metaconid DH (on the M_2, the distal crest does not connect directly on the distal part of the metaconid DH but at a short distance on the lingual marginal crest), delineating an oval-shaped basin. The C6 is expressed on the RM_2 in the form of a tiny DH visible on the marginal ridge of the distal fovea between the hypoconulid and entoconid DHs (Fig. 5). The C6 is well pronounced on the RM_3. In *P. paniscus*, we also note limited variation in mesial to distal expression of the EDJ trigonid crest (Fig. 5). From the RM_1 to the RM_3, we observe a different pattern than that found in *P. troglodytes,* in which a single, transverse crest links the protoconid and metaconid DH. On the M_1, we observe separate crests on the mesial slopes of the protoconid and metaconid DHs, which run for a short distance towards the occlusal basin. None of the *P. paniscus* specimens show any sign of a C6 (Fig. 5).

We plot the first two PCs in the analysis of changes in the configuration of semi-landmarks in order to reveal differences in shapes between mandibular molars within and between individuals. The first PC accounts for 47.6% of the variation, whereas the second and third PC account for 29.7 and 7.7%, respectively (Fig. 9). For both chimpanzees, PC1 separates 3D-EDJ within the same tooth row. Within each species, the Procrustes superimposition shows, from the M_1 to the M_3, a progressive buccolingual elongation of the 3D-EDJ, mainly at the level of the mesiolingual angle. Within each species, this metameric change in configuration is associated with a progressive flattening of the distal DH (Fig. 9). The inter-individual differences in 3D-EDJ shapes increase from the M_1 to the M_3. This is mainly due to the fact that, in the *P. paniscus* individual only, the metameric variation from the M_1 to the M_3 is indicated by higher scores on both PC1 and PC2. In the *P. troglodytes* specimen, the scores on PC2 for the M_1 range within the values obtained for the M_3 antimeres. In other words, the pattern of intra-individual metameric variation is not the same in the two chimpanzees sampled in this study. The Procrustes superimposition of the *P. troglodytes* RM_1 (CS = 24.5) and the right/left *P. paniscus* M_{1s} (CS = 22.1 for both teeth) shows a significant distal shift of the mesiolingual and distobuccal DH in the former (Fig. 9). The same trend is observed after the Procrustes superimposition of the *P. troglodytes* RM_2 (CS = 24.0) and the right/left *P. paniscus* M_2 (CS = 24.1 for both teeth), the *P. troglodytes* right/left M_3 (CS = 22.4 and 21.9, respectively) and the right/left *P. paniscus* M_3 (CS = 20.4 and 20.7, respectively). However, for both M_2 and M_3, the changes in shape configuration between the two species also correspond to a buccolingual constriction of the 3D-EDJs in *P. troglodytes*, as compared with *P. paniscus*. In *P. troglodytes*, the CS decreases from the M_1 to the M_3 (see above). In *P. paniscus*, the CS increases from the M_1 to the M_2 and then decreases from the M_2 to the M_3.

Antimeric metrical variation cannot be evaluated for the M_1 and M_2 of the *P. troglodytes* mandible. For all other molars, antimeric variation is limited and seems to be metrically (after Procrustes superimposition, Fig. 9) and morphologically higher on the M_3 (for both mandibles) than on the M_1 and M_2 (for the *P. paniscus* mandible).

The M_{1s} and M_{2s} in extant humans: within- vs. between-individual variation

For all M_1 as well as M_2 of the individual numbered 574, we are able to investigate changes of the 3D-EDJ and OES (Figs 2 and 6, Table 1) as these developing tooth germs are still embedded in bone. The M_2 of the individuals numbered 383 and 512 are represented only by their 3D-EDJ (Figs 2 and 6, Table 1) as their enamel caps have not been completely formed. We describe the right M_1 and M_2 3D-EDJ and OES (Figs 2 and 6) of these three mandibles representing extant humans. These right surface reconstructions are subsequently compared with the left ones (see Supporting Information).

The OES metameric M_1/M_2 variation is well known for extant humans and consists mainly of a five-cusped M_1 associated with a four-cusped M_2. This pattern of high metameric variation can be also seen on the 3D-EDJ of the three individuals sampled in this study (Fig. 6). In general, when data are available for a given tooth, we observe a close morphological correspondence between the 3D-EDJ morphology and the OES morphology (Fig. 6). Additional morphological intra-individual M_1/M_2 metameric variations can be recorded. For example, on individual Embr 383, the M_2 shows a continuous crest connecting the protoconid DH and the metaconid DH, whereas this crest is interrupted on the M_1 (Fig. 6). Another example of intra-individual morphological M_1/M_2 metameric variation is given with individual Embr 512 (male, 4 years and 6 months old). In the case of the 3D-EDJ and OES of the M_1, there is a crest connecting the metaconid DH and the hypoconid DH. Such a crest is not recorded on the M_2 (Fig. 6).

When we investigate 3D-EDJ variations in extant humans, we plot only the first two PCs in the analysis of changes in

the configuration of semi-landmarks in order to reveal differences in shapes between M_{1s} and M_{2s} after Procrustes superimposition (Fig. 10). The first PC accounts for 43.8% of the variation, whereas the second and third PCs account for 27.0 and 10.2%. For each tooth the antimeric morphological variation and the dentine/enamel differences are limited in the sense that they never exceed metameric or inter-individual variation. For all three individuals, the CS decreases from the right/left M_{1s} to the right/left M_{2s} (Embr 383: from 23.6 and 23.4, respectively, to 20.1 on both sides; Embr 512: from 22.9 and 22.8, respectively, to 19.5 and 19.9; Embr 574: from 20.2 on both sides to 19.4 and 19.9, respectively). The morphological inter-individual differences appear larger for the M_2 than for the M_1. For example, the M_2 of individuals 383 and 512 appears much more different on PC1 than their M_1. Moreover, the M_1 vs. M_2 metameric variation of the 3D-EDJ varies greatly from one individual to another. Indeed, the M_1 and M_2 of individual 512 show much more difference on PC1 than those of individual 383. For individual 512, the M_1 to M_2 changes in configuration correspond to an important enlargement of the distobuccal angle, associated with a reduction of the mesiolingual angle and the absence of the hypoconulid DH (Figs 6 and 10). As opposed to the M_1, with its more or less quadrangular occlusal outline, the M_2 appears more triangular in occlusal view (Fig. 6). For individual 383, the M_1 to M_2 changes in configuration of the ED-EDJs are less visible even if they also correspond to an enlargement of the distobuccal angle associated with the absence of the hypoconulid DH, but to a much lesser extent (Figs 6 and 10). Moreover, the M_1 and M_2 of individual 574 show some morphological differences, but on PC2 rather than on PC1. In this case, not surprisingly, the M_1 to M_2 changes in configuration of the ED-EDJ correspond to the absence of the hypoconulid DH associated with a small constriction of the distal part of the surface (Figs 6 and 10). If we now compare within- vs. between-individual metameric variation of the 3D-EDJ, we observe interesting results (Fig. 10). For example, the M_1 of individual 574 and the M_2 of individual 383 group well together on both PC1 and PC2. They appear much closer in shape than the M_1 of individual 383 and the M_2 of individual 574, which clearly separate on both PC1 and PC2. Surprisingly, for individual 574 (female, 5 years and 4 months old), the M_1 is closer in shape to that of the M_2 of individual 383 than to its own M_2. In other words, within the three extant humans sampled so far, inter-individual 3D-EDJ M_1/M_2 metameric variation varies greatly but intra-individual metameric variation can be greater even than inter-individual metameric variation.

The antimeric M1/M2 morphological (see Supporting Information) and metrical (after Procrustes superimposition) variation is limited. Differences in CS are very small, if any, for both 3D-EDJ and OES. No right/left antimeric difference in CS of the OES can be seen on the M_1 of individual Embr 383 (26.9) and only small differences in CS can be reported for individuals Embr 512 (26.5 and 26.9, respectively) and Embr 574 (23.3 and 23.5, respectively). This right/left antimeric difference in CS of the OES appears slightly higher on the M_2 of individual Embr 574 (23.2 and 24.2, respectively).

The mandibular postcanine row: differences in patterns between species

After separate investigation of metameric variation of the 3D-EDJs within Sts 52, extant humans and chimpanzees, we plotted the first three PCs in the analysis of changes in the configuration of semi-landmarks in order to determine whether the Sts 52 pattern of 3D-EDJ mandibular metameric variation is common and can be grouped with that observed in extant humans, chimpanzees or both.

The first PC accounts for 27.6% of the variation, whereas the second, third and fourth PCs account for 18.9, 17.4 and 7.6%, respectively (Fig. 11). After Procrustes superimposition, intra-individual 3D-EDJ mandibular metameric variation appears in all six mandibles investigated. At first glance, the metameric pattern of mandibular molar variation appears much smaller within each of the two chimpanzee mandibles as compared with the intra-individual pattern observed in extant humans. Moreover, the *P. paniscus* mandible displays less metameric variation than the *P. troglodytes* on PC3. Surprisingly, even the inter-individual (inter-specific) metameric pattern observed between the two chimpanzee mandibles sampled in this study appears much smaller than the extant human intra-individual metameric pattern. The pattern of mandibular molar metameric variation seen in Sts 52 appears much smaller than (on PC1) or equivalent to (on PC2 and PC3) the intra-individual pattern observed in extant humans. Moreover, the Sts 52 pattern appears greater than that observed within each of the two chimpanzee mandibles but not greater than that found between the two chimpanzees. In other words, the fossil hominin examined in this study, representing *A. africanus* (Sts 52), displays a relatively small metameric pattern on PC1, PC2 and PC3, much more similar to that seen between the two chimpanzee mandibles than either the intra-individual or inter-individual patterns observed in the three extant humans sampled so far. When we examine the values of the 3D (non-projected) five mandibular angles selected on the apices of the main DHs, we observe that the lowest metameric variation always occurs at the protoconid level in Sts 52, chimpanzees and extant humans (Fig. 12 and Supporting Information).

Discussion

The purpose of the present study was to analyse 3D changes in the expression of EDJ metrical and morphological features of an *A. africanus* individual's (Sts 52) entire mandibular and maxillary postcanine dentition, thereby investigating intra-individual variability. No previous study

has attempted to analyse intra-individual morphological and metrical variation at the EDJ in a fossil hominin specimen. *A. africanus* displays ''the most unusual pattern of variation'' (Kimbel & White, 1988) reported in any Pliocene or Plio-Pleistocene hominin species, a large degree of morphological variation well manifested in the face. Sts 52 illustrates the degree of polymorphism seen in the facial skeleton of *A. africanus*. For this species, Kimbel & Rak (1993) listed nine diagnostic facial derived characters and noticed that Sts 52, ''the least prognathic *A. africanus* cranium'' (Kimbel & White, 1988), was more generalized in lacking two out of these nine features: the anterior pillars and maxillary furrows. Our study did not aim to describe the postcanine morphological pattern of the 3D-EDJ of Sts 52 as a single reference for all of the *A. africanus* representatives. The questions addressed in this study are simple: does the expression of a morphological and/or metrical trait on a given 3D-EDJ of Sts 52 exactly predict the expression of the same trait on another tooth of the same class and quadrant, and how can we interpret the observed metameric variation using a comparative sample of extant humans and chimpanzees?

As revealed by the analysis of morphological features, registration and PC analysis, we found that the intra-individual metameric premolar variation was strong, whereas antimeric premolar variation was faint for both maxillary and mandibular quadrants. With regard to the mandibular row, Hillson (1996) considered that, in the lower P_4, three-cusped forms dominate in *Australopithecus* (but two-cusped forms can be found), whereas *Paranthropus* usually has two main cusps. To our knowledge, a new 3D-EDJ character was recorded on both right and left 3D-EDJ P_{4s}: the distolingual occlusal accessory ridge on the lingual part of the distal fossa. This morphological feature was not recorded on the P_3. Further observations on other mandibular premolar 3D-EDJs will be needed to determine whether the distolingual occlusal accessory ridge is a distinctive feature of *A. africanus* P_4. With regard to the maxillary row, the P^3 is distinct (on both sides) in showing its mesial buccal groove delimited on its outer margin by a cingulum-like ridge. Robinson (1956) noticed the presence in all of the Sterkfontein maxillary OES of premolars available at his time of ''a thickened cingulum-like ridge…forming a raised margin round the buccal face except for the occlusal margin'' (p. 58). He concluded that this condition was ''not known on any *Paranthropus* P^3'' (op. cit., p. 58). Whether the distolingual occlusal accessory ridge on the P_4 and the cingulum-like ridge on the mesial buccal face on the P^3 simply represent individual morphological variations at the EDJ or taxonomically or evolutionarily relevant anatomical features needs to be determined by further investigations on other complete premolar rows in *A. africanus* and other Pliocene hominin species. As for the premolars, we found that the intra-individual metameric molar variation was much higher than the antimeric molar variation for both maxillary and mandibular quadrants. The protostylid expression has been considered to distinguish *A. africanus* and *P. robustus* (Skinner, 2008a; Skinner et al. 2009). Our observations on the metameric variation of Sts 52 in the protostylid expression confirm the description of Skinner et al. (2008a, 2009) of what he believed to represent the *A. africanus* condition. Indeed, on the first, second and third mandibular molars of Sts 52, the protostylid crest-like structures at the EDJ extend mesially of the protoconid DH (Fig. 3). As the OES of the mandibular and maxillary first permanent molars of Sts 52 is worn flat to the point where the DHs are also slightly worn, we could not compare the height of DHs between M_1 and M_2. However, significant differences in the height of the DHs are found between the M_2 and M_3, with a lowering of the buccal DHs (both protoconid and hypoconid) in the latter. This observation corresponds only in part to the observations on isolated mandibular molars representing different individuals of Skinner (2008b), who reported an increase in the height of the mesial DHs and a decrease in the height of the distal DHs on the M_3 compared with the M_2. Differences in results might be due to either differences in registration methods or the nature of the variation reported, which in the present study is metameric *stricto sensu*, i.e. intra-individual. Our results indicate that the main changes due to intra-individual metameric variation is only partly expressed in the height of the DHs but also in the local increase of specific areas of the 3D-EDJ (e.g. on the mandibular molars, the increase of the mesiolingual and distobuccal angles) and in the relative height of the marginal ridges (e.g. on the mandibular molars, the sagging of the mesial marginal ridge, relative to the situation of the trigonid crest; on the maxillary molars, the sagging of the distal marginal ridge). The results on Sts 52 showed that both patterns of antimeric and metameric variations are of the same magnitude between the mandibular and maxillary arcades. Antimeric variation on Sts 52 also tends to be of the same magnitude between key teeth and their distal counterparts among each postcanine class.

The pattern of intra-individual 3D-EDJ metameric variation observed on the mandibular molars of Sts 52 was compared, firstly, with the extant human patterns of within- vs. between-individual metameric variation of M_1 and M_2 and, secondly, with the chimpanzee patterns of intra-individual metameric variation of mandibular molars. No previous study has attempted to investigate within- vs. between-individual morphological and metrical variation at the EDJ in three dimensions in a sample of extant humans and chimpanzees. We observed that the pattern of intra-individual metrical metameric variation was not the same in the *P. paniscus* and *P. troglodytes* mandibles sampled in this study as the differences in 3D-EDJ shapes between individuals increased from the M_1 to the M_3 (Fig. 9). The metameric pattern observed between the two chimpanzee mandibles appeared much smaller than the extant human

intra-individual metameric pattern (Fig. 11). Among the three extant humans sampled so far, the 3D-EDJ M_1/M_2 metameric variation between individuals varied greatly and, importantly, this metameric variation was even greater within individuals than between individuals (see e.g. individuals Embr 383 and Embr 574; Fig. 10). In extant humans, the differences in shapes between the 3D-EDJ appeared larger for the M_2 than for the M_1.

The results of the present exploratory study demonstrate that 3D-EDJ shape variation is high and complex as the metameric differences in shapes, within the same species and/or genus, can vary from one individual to another and can therefore mask differences between taxa (Fig. 11). Previous studies have already investigated metameric variation in primate molar OES or cross-sections of EDJ (e.g. Hlusko, 2002; Smith et al. 2006; Olejniczak et al. 2007) but none have attempted to distinguish within- vs. between-individual differences. We believe that differences in results might be due to the fact that we carefully distinguished the within- vs. between-individual components of metameric variation. Another difficulty was that all previous studies investigated either 2D metameric variation at the OES (Hlusko, 2002) or metameric cross-sectional differences in *Papio ursinus* maxillary molars (Olejniczak et al. 2007) and extant human molars (Smith et al. 2006). Differences in results might also be due to the fact that we did not investigate the configurations of small sets of landmarks in cross-sections of teeth or on 2D images but, instead, we tried to capture the complex changes of the EDJ in three dimensions by using larger sets of 3D points and by combining analyses of shape changes with observations on morphologically 'discrete' (non-metrical) features, which has proven to be of taxonomic value for the hominoid OES (Uchida, 1992) and hominoid skull (Braga, 1995, 1998; Braga & Boesch, 1997a,b).

It has long been known that the expression of a particular morphological trait on one tooth of a class is dependent on trait expression on other types of the class. Such cases where a single trait is expected on types of the same class have been called within-field interactions (Dahlberg, 1945) and can be associated with the concept of dental morphological/developmental integration or modularity (Raff, 1996) as applied to dental development by Braga & Heuzé (2007). However, our results show that the expression of a trait on a given 3D-EDJ of either a chimpanzee, fossil hominin (Sts 52) or extant human does not necessarily predict the expression of the same trait on another 3D-EDJ of the same class and quadrant. This is already known at the OES for both extant primates and fossil hominins.

The fossil hominin examined in this study, Sts 52, shows a metameric pattern of mandibular variation in shape that is comparable to the pattern seen between the two chimpanzee mandibles. This degree of metameric variation appears relatively small as compared with the much larger patterns of variation in shapes observed between extant humans and even within them (Fig. 11). However, for some morphological features (e.g. the trigonid crest), Sts 52 shows a metameric pattern that is high. A high degree of morphological metameric variation can also be seen in extant humans (Fig. 6). The intra-individual metametic morphological and metrical variation of the 3D-EDJ will require further research to determine if it operates in the context of an integrated system. In other words, we will need more data on other complete specimens (either for mandibular or maxillary rows) to determine the patterns of covariation of the same given trait between the teeth of the same class and quadrant, and also the patterns of covariation in a set of traits within each tooth of a given class. To address this question we will also need new (and, preferably, automatic) methods to quantify more precisely all of the local changes observed between the 3D polygonal models (triangle-based, surfaces or meshes). At this stage, it has been demonstrated that most dental morphological traits are dependent from each other and that they have the developmental potential for correlated changes during evolution (Kangas et al. 2004). More recently, Braga & Heuzé (2007) proposed and defined a hypothesis of modularity in the human dental system, in which the developing canines, premolars and molars were considered to covary as a hierarchical unit during evolution, arising primarily by strong connections between developmental pathways. Their method derived from this concept (Braga & Heuzé, 2007) can be used as a basis for identifying and studying patterns of dental growth during the course of human evolution.

The findings of the present study of Sts 52, with a metameric pattern more similar to that of the two chimpanzees than to that of the three extant humans represented in our sample, correspond well to the findings and conclusion of Hlusko (2002) that ''the distinctive modern human [metameric] pattern had not evolved yet in the hominids from Sterkfontein [including Sts 52]'' (p. 95). She argued that differences in metameric patterns may not result from modifications of developmental mechanisms but rather from functional constraints.

The EDJ topography is often interpreted in terms of functional adaptations and might reflect adaptive capabilities of teeth to efficiently process tough items (Suwa et al. 2007). No studies have been carried out to test this functional hypothesis. According to the current masticatory biomechanical models, two causal factors could be considered. The first might occur over evolutionary time and the second might occur during the time span of dental morphogenesis. In this latter case, at early stages of dental development, the epithelial/mesenchymal interface (the common plane from which ameloblasts and odontoblasts move in opposite directions during odontogenesis) could sense mechanical stimuli and react to these through the molecular mechanisms of mechanotransduction (Tschumperlin et al. 2004). Further study is needed before the exact process (developmental and/or natural selection) responsible for the mechanical design of the 3D-EDJ is identified.

Summary conclusions

We conclude that the pattern of intra-individual 3D-EDJ metameric variation in shape is different in one *P. paniscus*, one *P. troglodytes* and three extant human mandibles sampled in this exploratory study. The metameric pattern observed between the two chimpanzee mandibles is much smaller than that found in the extant human intra-individual metameric pattern. The 3D-EDJ shape metameric variation is high and complex as the morphological and metrical differences within the same species and/or genus can vary from one individual to another and can therefore mask differences between taxa. Importantly, the 3D-EDJ metameric variation in extant humans can be greater within individuals than between individuals, with differences in shapes appearing larger for the M_2 than for the M_1. We found that the fossil hominin examined in this study, Sts 52, representing *A. africanus*, shows a metameric pattern of mandibular shape variation that is comparable to the pattern seen in two chimpanzees. This degree of metameric variation appears relatively small as compared with the much larger patterns of variation observed within and between extant humans.

From these observations of the 3D-EDJ in mandibular and maxillary postcanine teeth of one *A. africanus* specimen, two chimpanzees (*P. paniscus* and *P. troglodytes*) and three extant human mandibles, we recommend the use of a new approach in which within and between metameric variation is systematically assessed on securely identified members of a morphological class before making inferences about differences between fossil hominin species, using isolated teeth representing different individuals.

From our observations of Sts 52, we suggest that taxonomically relevant anatomical features may be represented on the premolar EDJ, including the P_4 antimeres (the disto-lingual occlusal accessory ridge) and the P^3 antimeres (the cingulum-like ridge on the mesial buccal face). This needs to be tested by further investigations on other complete premolar rows in *A. africanus* and other Plio-Pleistocene hominin species.

Acknowledgements

This study was supported by the French Ministry of Foreign Affairs, the HOPE Programme supported by the French Embassy in South Africa, the National Research Foundation (South Africa), the Centre National de la Recherche Scientifique (PEPS-ODENT Programme) and the European Commission Marie Curie Research Training Network (European Virtual Anthropology Network; http://www.evan.at), according to the Contract MRTNCT-2005-019564 (FP6). We thank Ms Stephany Potze, curator (paleontology department) at the Transvaal Museum (Pretoria, South Africa), and Dr Emmanuel Gilissen, curator (mammal department) at the Royal Museum of Central Africa (Tervuren, Belgium). We thank Audrey Berthier and Laurent Braak from the Institut de Médecine et de Physiologie Spatiales (Toulouse, France).

References

Besl P, McKay N (1992) A method for registration of 3-D shapes. *IEEE Trans Pattern Anal Mach Intell* **14**, 239–256.

Braga J (1995) Emissary canals in the Hominoidea and their phylogenetic significance. *Folia Primatol* **65**, 144–153.

Braga J (1998) Chimpanzee variation facilitates the interpretation of the incisive suture in South African Plio-Pleistocene hominids. *Am J Phys Anthropol* **105**, 121–135.

Braga J, Boesch C (1997a) Further data about venous channels in South African Plio-Pleistocene hominids. *J Hum Evol* **33**, 423–447.

Braga J, Boesch C (1997b) The ''radiator'' bias, Reply to Falk and Gage. *J Hum Evol* **33**, 503–506.

Braga J, Heuzé Y (2007) Quantifying variation in human dental developmental sequences. An EVO-DEVO perspective. In *Dental Perspectives on Human Evolution: State of the Art Research in Dental Anthropology* (eds Bailey S, Hublin JJ), pp. 245–259. Vertebrate Paleobiology and Paleoanthropology Series. Berlin: Springer.

Butler PM (1956) The ontogeny of molar pattern. *Biol Rev* **31**, 30–70.

Corruccini RS (1987) The dentinoenamel junction in primates. *Int J Primatol* **8**, 99–114.

Corruccini RS (1998) The dentino-enamel junction in primate mandibular molars. In *Human Dental Development, Morphology, and Pathology: A Tribute to Albert A. Dahlberg* (ed. Lukacs JR), pp. 1–16.Portland: University of Oregon Anthropological Papers.

Cowin SC, Moss ML (2001) Mechanosensory mechanisms in bone. In *Bone Mechanics Handbook*, 2nd edn (ed. Cowin SC), pp. 1–17. Boca Raton: CRC Press.

Dahlberg AA (1945) The changing dentition of man. *J Am Dent Assoc* **32**, 676–690.

Dart RA (1925) *Australopithecus africanus*: the man-ape of South Africa. *Nature* **115**, 195–199.

Hillson S (1996) *Dental Anthropology*. Cambridge: Cambridge University Press.

Hlusko L (2002) Identifying metameric variation in extant hominoid and fossil hominid mandibular molars. *Am J Phys Anthropol* **118**, 86–97.

Kangas AT, Evans AR, Thesleff I, et al. (2004) Nonindependence of mammalian dental characters. *Nature* **432**, 211–214.

Kimbel WH, Rak Y (1993) The importance of species taxa in paleoanthropology and an argument for the phylogenetic concept of the species category. In *Species, Species Concepts, and Primate Evolution* (eds Kimbel WH, Martin LB), pp. 461–484. New York: Plenum Press.

Kimbel WH, White TD (1988) Variation, sexual dimorphism and the taxonomy of *Australopithecus*. In *Evolutionary History of the ''Robust'' Australopithecines* (ed. Grine FE), pp. 175–192.New York: Aldine de Gruyter.

Koenderink JJ, van Doorn AJ (1992) Surface shape and curvature scales. *Image Vis Comput* **10**, 557–564.

Korenhof CAW (1960) *Morphogenetical Aspects of the Human Upper Molar*. Utrecht: Uitgeversmaatschappij Neerlandia.

Korenhof CAW (1961) The enamel–dentine border: a new morphological factor in the study of the (human) molar pattern. *Proc Koninkl Nederl Acad Wetensch* **64B**, 639–664.

Kraus BS (1952) Morphologic relationships between enamel and dentin surfaces of lower first molar teeth. *J Dent Res* **31**, 248–256.

Massler M, Schour I (1946) The appositional life span of the enamel and dentine-forming cells. I. Human deciduous teeth and first permanent molars. *J Dent Res* **25**, 145–150.

O'Higgins P (2000) Quantitative approaches to the study of craniofacial growth and evolution: advances in morphometric techniques. In *Development, Growth and Evolution: Implications for the Study of Hominid Evolution* (eds O'Higgins P, Cohn M), pp. 163–185. London: Academic Press.

Olejniczak AJ, Gilbert CC, Martin LB, et al. (2007) Morphology of the enamel–dentine junction in sections of anthropoid primate maxillary molars. *J Hum Evol* **53**, 292–301.

Raff RA (1996) *The Shape of Life: Genes, Development and the Evolution of Animal Form*. Chicago: University of Chicago Press.

Robinson JT (1956) The dentition of the Australopithecinae. *Transvaal Mus Mem* **9**, 1–179.

Schour I, Massler M (1940) Studies in tooth development. The growth pattern of the human teeth. *J Am Dent Assoc* **27**, 1778–1793, 1918–1931.

Scott GR, Turner CG (1997) *The Anthropology of Modern Human Teeth. Dental Morphology and its Variation in Recent Human Populations*. Cambridge: Cambridge University Press.

Skinner MM, Wood BA, Boesch C, et al. (2008a) Dental trait expression at the enamel–dentine junction of lower molars in extant and fossil hominids. *J Hum Evol* **54**, 173–186.

Skinner MM, Gunz P, Wood BA, et al. (2008b) Enamel–dentine junction (EDJ) morphology distinguishes the lower molars of *Australopithecus africanus* and *Paranthropus robustus*. *J Hum Evol* **55**, 979–988.

Skinner MM, Wood BA, Hublin JJ (2009) Protostylid expression at the enamel–dentine junction and enamel surface of mandibular molars of *Paranthropus robustus* and Australopithecus africanus. *J Hum Evol* **56**, 76–85.

Smith TM, Olejniczak AJ, Reid DJ, et al. (2006) Modern human molar enamel thickness and enamel–dentine junction shape. *Arch Oral Biol* **51**, 974–995.

Suwa G (1988) Evolution of the ''robust'' australopithecines in the Omo succession: Evidence from mandibular premolar morphology. In *Evolutionary History of the ''Robust'' Australopithecines* (ed. Grine FE), pp. 199–222. New York: Aldine de Gruyter.

Suwa G, Kono R, Katoh S, et al. (2007) A new species of great ape from the late Miocene epoch in Ethiopia. *Nature* **448**, 921–924.

Tschumperlin DJ, Dai G, Maly IV, et al. (2004) Mechanotransduction through growth-factor shedding into the extracellular space. *Nature* **429**, 83–86.

Turner CG, Nichol CR, Scott GR (1991) Scoring procedures for key morphological traits of the permanent dentition: the Arizona State University dental anthropology system. In *Advances in Dental Anthropology* (eds Kelley MA, Larson CS), pp. 13–31. New York: Wiley Liss.

Uchida A (1992) *Intra-Species Variation among the Great Apes. Implications for Taxonomy of Fossil Hominoids*. PhD Thesis, Harvard University.

Weiss KM (1990) Duplication with variation: metameric logic in evolution from genes to morphology. *Yrbk Phys Anthropol* **33**, 1–23.

Wood BA, Abbott SA (1983) Analysis of the dental morphology of Plio-Pleistocene hominids. I. Mandibular molars: crown area measurements and morphological traits. *J Anat* **136**, 197–219.

Wood BA, Abbott SA, Graham SH (1983) Analysis of the dental morphology of Plio-Pleistocene hominids. II. Mandibular molars – study of cusp areas, fissure patterns and cross sectional shape of the crown. *J Anat* **137**, 287–314.

Supporting Information

Additional Supporting Information may be found in the online version of this article.

Fig. S1. Mandibular antimeric variation illustrated on Sts 52 3D-EDJs.

Fig. S2. Maxillary antimeric variation illustrated on Sts 52 EDJs.

Fig. S3. Mandibular molar antimeric variation illustrated on two chimpanzee (*Pan troglodytes* and *Pan paniscus*) 3D-EDJs.

Fig. S4. Mandibular 3D-EDJ M_1/M_2 antimeric variation and M_1 3D-EDJ/OES differences illustrated on two extant humans.

Fig. S5. Mandibular 3D-EDJ M_1/M_2 antimeric variation; M_1 and M_2 3D-EDJ/OES differences illustrated on one extant human.

Fig. S6. Mandibular metameric variation of the premolar EDJs of a pygmy chimpanzee (*Pan paniscus*) and a common chimpanzee (*Pan troglodytes*).

Table S1. 3D non-projected angles (in degrees) measured at the level of the apices of the main DHs on the mandibular molars (Prt, Protoconid; Hyp, Hypoconid; Ent, Entoconid; Met, Metaconid; Hyld, Hypocolunid).

As a service to our authors and readers, this journal provides supporting information supplied by the authors. Such materials are peer-reviewed and may be reorganized for online delivery but are not copy-edited or typeset. Technical support issues arising from supporting information (other than missing files) should be addressed to the authors.